Model-Based Acceleration Thresholds for Longitudinal Wheel Slip Detection and Control

Akshay Kaundinya
Department of Mechanical Engineering
University of Michigan
Ann Arbor, Michigan 48109

***Abstract*—Traditional active automotive safety systems, such as Traction Control Systems (TCS), mainly rely on the longitudinal slip ratio to maximize tire-road transmissible force. However, calculating the slip ratio requires accurate estimation of the vehicle's true longitudinal ground speed, which introduces significant unreliability and mathematical singularities during all wheel slip or low-speed events. This paper presents a robust, velocity-independent traction control strategy using model-based wheel angular acceleration thresholds. To establish physically accurate limits, a 5-Degree-of-Freedom (5-DoF) longitudinal half-car model is derived, explicitly coupling pitch and bounce dynamics with a nonlinear Pacejka tire model to capture the effects of dynamic load transfer. Because numerical differentiation of discrete wheel speed sensor data drastically amplifies high-frequency noise, a novel three-stage discrete-time signal processing pipeline is introduced. By cascading a Kinematic Kalman Filter, a Causal Savitzky-Golay filter, and a Statistical Shrinkage Estimator, a clean acceleration signal is extracted without introducing prohibitive phase lag. Finally, a decentralized, asymmetric Proportional-Integral (PI) controller featuring an anti-windup clamp and slew-rate limiting is implemented. Simulation results across both Rear-Wheel Drive (RWD) and All-Wheel Drive (AWD) configurations on low-friction surfaces demonstrate that the proposed architecture successfully mitigates deep four-wheel slip events, relying solely on wheel angular velocity sensors.**

***Index Terms*—Traction Control Systems (TCS), Wheel Angular Acceleration, Velocity-Independent Control, Vehicle Dynamics, Pacejka Tire Model, Dynamic Load Transfer, Kinematic Kalman Filter, Savitzky-Golay Filter, Proportional-Integral (PI) Control, Slew-Rate Limiting, Active Safety Systems.**

I. Introduction

THE active control of longitudinal vehicle dynamics is a key segment of modern automotive safety and performance. Systems such as Traction Control (TCS) and Anti-lock Braking (ABS) are fundamentally designed to maximize the transmissible force between the tire and the road by keeping the longitudinal tire slip within an optimal range. Traditionally, these control systems rely on calculating the longitudinal slip ratio, a metric that requires accurate estimates of both the wheel angular velocity and the vehicle's true longitudinal ground speed [1].

However, relying on the slip ratio introduces a significant vulnerability into the control loop. During severe dynamic events, such as deep acceleration slip or simultaneous four-wheel slipping on low-friction surfaces (e.g., ice or snow), non-driven reference wheels may not be able to provide a reliable speed estimate. While advanced estimators using inertial measurement units (IMUs) or GPS can mitigate this, they introduce cost and complexity. As such, there is a clear need for simple slip detection and mitigation methods that operate independently of longitudinal vehicle velocity.

An alternative approach is the use of model-based wheel angular acceleration thresholds. Governed by the rotational dynamics of the wheel assembly, there exists a physical limit to the angular acceleration a wheel can sustain under maximum available road friction. If the applied powertrain torque induces an angular acceleration that exceeds this theoretical threshold, it definitely indicates that the tire has surpassed its peak tractive capability and has entered an unstable slip regime. This method allows for slip detection relying solely on wheel speed sensor data, bypassing the need for vehicle speed estimation entirely.

Despite its theoretical advantages, implementing an acceleration-based detection strategy presents a critical signal processing challenge. Standard vehicular wheel speed data, typically gathered via variable reluctance or Hall-effect sensors, is inherently discrete and subject to quantization error and electrical noise [2]. Deriving angular acceleration requires the numerical differentiation of this noisy speed signal, a process that inherently amplifies high-frequency noise and can lead to false-positive slip detections or erratic controller behavior.

This project investigates the development of a robust, acceleration-threshold-based longitudinal slip controller. A key area of focus is on the signal processing pipeline, specifically evaluating trade-offs between various discrete-time filtering methods to achieve a clean acceleration signal without introducing prohibitive phase lag. Using a dynamic vehicle and nonlinear tire model, the proposed detection logic and subsequent torque-reduction control strategy are evaluated across varying friction conditions to demonstrate the viability of velocity-independent traction control.

II. Vehicle Dynamics

To accurately evaluate the proposed acceleration-based slip detection logic, a dynamic vehicle model is required. While kinematic models can describe steady-state behavior, they fail to capture the transient response present during severe acceleration and low-friction slip events. Therefore, a 5-Degree-of-Freedom (5-DoF) vehicle (half car) model was used to capture the essential longitudinal, vertical, and rotational dynamics of the system.

The system's five degrees of freedom comprise the longitudinal vehicle position (x), the bounce of the chassis (y), the pitch of the chassis (θ), and the independent rotational angles of the two axles (θ_F and θ_R). As illustrated in Figure 1, the sprung mass (m, J) is connected to the front and rear unsprung wheel masses (m_F and m_R) via a suspension system modeled with linear spring stiffness (k_F, k_R) and damping (c_F, c_R) coefficients.

The inclusion of the bounce and pitch dynamics is critical for this study due to the phenomenon of dynamic load transfer. Longitudinal acceleration induces a load shift from the front to the rear axle, continuously altering the normal forces acting on the contact patches. Because the peak transmissible tractive force is highly sensitive to these instantaneous normal loads, accurately simulating the suspension dynamics is a prerequisite for establishing reliable, physical wheel angular acceleration thresholds. The rotational dynamics of each wheel are subsequently driven by the applied powertrain torque, brake torque, and the opposing longitudinal tire force generated at the road interface.

A. Model Diagram

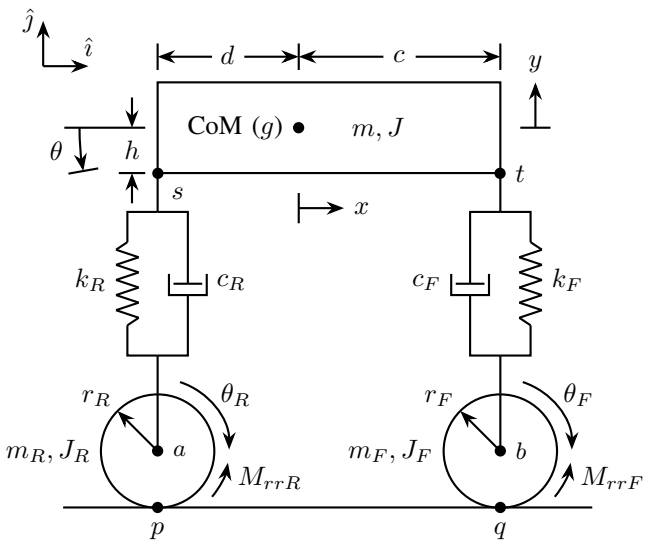


Fig. 1. 5-DoF Longitudinal Half-Car Vehicle Model. p_R and p_F are points on the wheel.

B. Kinematics and System Energies

To formulate the equations of motion, the body-fixed chassis frame is resolved into the global inertial frame using a pitch rotation matrix. Assuming the road surface is at $y = 0$ and that each suspension link remains perpendicular to the road surface, the absolute vertical bounce of the chassis at the front and rear suspension mounting locations are extracted kinematically as $y_t = y + c\sin\theta - h\cos\theta$ and $y_s = y - d\sin\theta - h\cos\theta$, respectively.

The system dynamics are derived using the Lagrangian approach. The total potential energy (V), kinetic energy (T), and Rayleigh Dissipation Function (D) are formulated to capture the translational, vertical, pitch, and independent wheel rotational energies, alongside the elastic and dissipative forces of the linear suspension springs and dampers.

Finally, the generalized non-conservative forces acting on the system are determined using the Principle of Virtual Power ($\delta P = \sum \vec{F} \cdot \delta\vec{v}$). These external forces include aerodynamic drag ($\vec{F}_{drag}$), applied powertrain and braking torques (M_F, M_R), wheel rolling resistance, and the longitudinal tire friction forces ($\vec{F}_F, \vec{F}_R$) acting at the contact patches.

C. Equations of Motion via Lagrange's Formulation

With the system energies and virtual power established, the equations of motion are derived using Lagrange's equations of the second kind. Evaluating the formulation yields the five coupled, nonlinear equations governing the vehicle's degrees of freedom (assuming a small-angle approximation for pitch, θ):

$$\ddot{x} = \frac{F_{xF} - F_{drag} + F_{xR}}{m + m_F + m_R} \tag{1}$$

$$\begin{aligned}\ddot{y} = {} & \frac{k_R(h - y + d\theta)}{m} - \frac{k_F(y - h + c\theta)}{m} - g \\ & - \frac{c_F(\dot{y} + c\dot{\theta} + h\theta\dot{\theta})}{m} - \frac{c_R(\dot{y} - d\dot{\theta} + h\theta\dot{\theta})}{m}\end{aligned} \tag{2}$$

$$\begin{aligned}\ddot{\theta} = {} & \frac{F_{xF}(h - c\theta) + F_{xR}(h + d\theta)}{J} \\ & - \frac{c_F(c + h\theta)(\dot{y} + c\dot{\theta} + h\theta\dot{\theta})}{J} \\ & + \frac{c_R(d - h\theta)(\dot{y} - d\dot{\theta} + h\theta\dot{\theta})}{J} \\ & - \frac{k_F(c + h\theta)(y - h + c\theta)}{J}\end{aligned} \tag{3}$$

$$\ddot{\theta}_R = \frac{M_R - F_{xR}r_R - \mu_{Rr}F_{yR}r_R}{J_R} \tag{4}$$

$$\ddot{\theta}_F = \frac{M_F - F_{xF}r_F - \mu_{Fr}F_{yF}r_F}{J_F} \tag{5}$$

D. Dynamic Vertical Reaction Forces

To dynamically update the peak friction limit of the tire model, the instantaneous normal forces acting on the front and rear contact patches (F_{yF} and F_{yR}) must be evaluated. Assuming the unsprung wheel masses are constrained to move purely parallel to the road surface, their vertical accelerations are strictly zero.

By balancing the vertical free-body forces (upward road reaction, downward gravity, and internal suspension forces) acting on each unsprung mass, the explicit equations for the dynamic normal loads are extracted as:

$$F_{yF} = m_F g - k_F(y - h + c\theta) - c_F(\dot{y} + c\dot{\theta} + h\theta\dot{\theta}) \tag{6}$$

$$F_{yR} = m_R g + k_R(h - y + d\theta) - c_R(\dot{y} - d\dot{\theta} + h\theta\dot{\theta}) \tag{7}$$

E. Tire Dynamics and Longitudinal Slip

To accurately determine the non-conservative longitudinal tractive forces (F_{xF} and F_{xR}) acting on the vehicle, a non-linear tire model is required. The Pacejka "Magic Formula" is utilized for its ability to empirically map the non-linear relationship between tire slip and generated longitudinal force [3].

The fundamental input to the longitudinal Pacejka model is the longitudinal slip ratio (κ). Traditionally, acceleration slip is defined as the normalized difference between the rotational speed of the tire's contact patch and the true longitudinal ground speed of the wheel hub [3]. For the front and rear axles, let v_{bx} and v_{ax} denote the absolute longitudinal hub velocity, respectively:

$$v_{bx} = \dot{x} - c\dot{\theta}\theta + h\dot{\theta} \tag{8}$$

$$v_{ax} = \dot{x} + d\dot{\theta}\theta + h\dot{\theta} \tag{9}$$

The standard mathematical definition of the slip ratio during acceleration is evaluated as:

$$\kappa = \frac{\dot{\theta}r - v_x}{\dot{\theta}r} \tag{10}$$

To ensure simulation stability and accurately model deep slip events, this project utilizes the formula shown in (11). By replacing the denominator with the maximum of either the wheel speed or the hub speed, the slip ratio remains naturally bounded:

$$\kappa = \frac{\dot{\theta}r - v_x}{\max(\dot{\theta}r, \epsilon_{tol})} \tag{11}$$

where ϵ_{tol} is a small constant included to prevent a divide-by-zero condition when the vehicle is entirely stationary (or if the wheels are locked up), it is important to note that traditional Traction Control Systems fundamentally rely on estimating this highly sensitive κ parameter [1].

The base vehicle coordinate system and slip terminology adhere to the SAE J670 / ISO 8855 standards [4]. However, to ensure numerical stability around the zero-speed singularity during deep slip events, the simulation sets the denominator to the maximum of the rotational or a small ϵ_{tol}.

With the stabilized slip ratio κ calculated, the longitudinal tractive force F_x generated at each contact patch is determined via the Pacejka Magic Formula [3]:

$$F_x = D \sin\left[C \arctan(B\kappa - E(B\kappa - \arctan(B\kappa)))\right] \tag{12}$$

The geometric coefficients of the curve define the tire's transient response: $B = 10$ dictates the stiffness in the low-slip elastic region, $C = 1.9$ acts as a shape factor, and $E = 0.97$ controls the curvature near the tractive peak [5]. The peak factor D defines the absolute maximum transmissible force and is directly proportional to the instantaneous normal load acting on the tire ($D = \mu F_y$, where μ is the road friction coefficient) [3]. This explicitly couples the longitudinal tire dynamics to the vertical bounce (y) and pitch (θ) dynamics of the chassis, accurately capturing the reduction in front-axle tractive capability due to dynamic load transfer during hard acceleration.

III. Signal Processing and Noise Filtering

While the dynamic model establishes theoretical acceleration limits, implementing this strategy on physical hardware introduces a severe signal processing challenge. Deriving angular acceleration from discrete, noisy wheel speed sensors via standard numerical differentiation inherently amplifies high-frequency quantization noise, leading to false-positive slip detections. Conversely, applying heavy low-pass filters introduces phase delay, rendering rapid feedback control impossible. To extract a clean acceleration signal without prohibitive latency, a novel three-stage discrete-time processing pipeline was developed.

A. Kinematic Kalman Filter

The first stage applies a 3-State Kinematic Kalman Filter [6] to the raw wheel speed data. The state vector is defined as $x_k = \begin{bmatrix}\omega_k & \alpha_k & j_k\end{bmatrix}^T$, representing angular velocity, acceleration, and jerk. The discrete-time state transition matrix (A) is derived directly from fundamental rotational kinematics:

$$x_{k+1} = Ax_k = \begin{bmatrix}1 & \Delta t & \frac{\Delta t^2}{2} \\ 0 & 1 & \Delta t \\ 0 & 0 & 1\end{bmatrix} \begin{bmatrix}\omega_k & \alpha_k & j_k\end{bmatrix} \tag{13}$$

Because only velocity is measured, the measurement matrix is defined as $H = \begin{bmatrix}1 & 0 & 0\end{bmatrix}$.

The effectiveness of this filter rests on the deliberate tuning of its noise covariance matrices. The measurement noise covariance was set high ($R = 6$) to reflect electrical and quantization noise. The process noise covariance (Q) heavily penalizes the lower-order states while leaving the unmeasured jerk state relatively free:

$$Q = \begin{bmatrix}10^{-4} & 0 & 0 \\ 0 & 10^{-4} & 0 \\ 0 & 0 & q_{jerk}\end{bmatrix} \tag{14}$$

where $q_{jerk} = 50$. This permits the filter to rapidly adjust its acceleration estimate during transient slip events while forcing it to rely on its internal kinematic prediction model rather than noisy discrete measurements, effectively bypassing numerical differentiation.

B. Polynomial Smoothing and Shrinkage Estimation

To further smooth the estimated acceleration ($\hat{\alpha}_k$) without introducing the linear phase delay typical of Butterworth filters, the Kalman output is passed through a Causal Savitzky-Golay (SG) filter [7]. Operating in real-time, the filter fits a third-order polynomial to an 11-point moving window of recent estimates and extracts the causal endpoint value.

While the SG filter successfully removes mid-band noise, the causal endpoint evaluation introduces minor polynomial variance ("tail-wagging") at the boundaries. To mitigate this and ensure control stability, a final Statistical Shrinkage Estimator [8] is applied. The acceleration signal is pulled toward the local 10-point mean, formulated as $\alpha_{final} = \beta\alpha_{current} + (1 - \beta)\alpha_{mean}$, with a heavy bias of $\beta = 0.01$. This final stage drastically dampens limit-cycling in the torque reduction controller while maintaining an acceptable threshold-detection latency.

IV. Feedback Control Strategy

A. Proportional-Integral (PI) Regulation

With a filtered angular acceleration signal ($\hat{\alpha}$) established, a feedback control loop is required to maintain the wheel slip at the threshold of maximum tractive force. The error signal (e_k) is defined as the difference between the estimated angular acceleration and the model-based physical threshold (α_{target}):

$$e_k = \hat{\alpha}_k - \alpha_{target,k} \tag{15}$$

To minimize this error, a discrete-time Proportional-Integral (PI) controller was implemented to govern the torque reduction commanded to the powertrain. The control law evaluates the necessary torque reduction (ΔM) as:

$$\Delta M = \max\left(0, K_p e_k + K_i \sum_{j=1}^{k} e_j \Delta t\right) \tag{16}$$

where K_p and K_i represent the proportional and integral gains, respectively. The output is strictly clamped at zero to ensure the safety system only removes torque and never artificially increases the driver's torque demand.

A PI controller was selected due to its structural simplicity, low computational overhead, and established effectiveness in regulating first-order dynamic errors [9]. The proportional term provides an instantaneous reaction to abrupt threshold crossings, which is critical for suppressing rapid wheel spin, while the integral term eliminates steady-state error, ensuring the acceleration perfectly tracks the friction limit without persistent offset.

While advanced control methodologies, such as Model Predictive Control (MPC) or Sliding Mode Control (SMC), offer superior constraint handling and optimization capabilities [10], they require intensive real-time computation and highly accurate state estimation models. Given the project objective of developing a robust, velocity-independent system utilizing minimal sensor data, the PI framework proved exceptionally effective and computationally efficient. Nevertheless, there remains room for future optimization, and implementing adaptive gain scheduling or robust non-linear techniques could further improve the transient response across rapidly changing "μ-jump" scenarios.

B. Asymmetric Intervention and Slew-Rate Limiting

A pure PI implementation acting on a highly non-linear plant, such as the Pacejka tire model, is inherently prone to high-frequency limit cycling, often manifesting as "bang-bang" chatter. When the control intervention instantaneously returns torque to the drivetrain upon dropping below the slip threshold, the tire breaks traction again in a rapid, repetitive cycle. At frequencies exceeding $10\,\text{Hz}$, this oscillation induces severe mechanical shock and driveline fatigue [11].

To mitigate this destructive chatter, two critical modifications were integrated into the control architecture. First, an integral anti-windup clamp was applied to prevent the accumulation of massive negative error during standard, non-slipping operation. Second, an asymmetric slew-rate limiter was implemented on the torque recovery phase. While the controller is permitted to cut torque instantaneously to suppress slip, the rate at which torque is returned to the driver is strictly bounded by a maximum physical recovery rate ($\dot{M}_{max}$):

$$\Delta M_k = \max(\Delta M_{k-1} - \dot{M}_{max}\Delta t, \Delta M_{raw}) \tag{17}$$

This ensures that the torque interventions smoothly respect the mechanical inertia of the powertrain, transforming violent high-frequency chatter into controlled, low-amplitude limit cycles that safely maximize continuous longitudinal acceleration.

V. Results and Discussion

A. Sensor Noise and Filtering Pipeline Validation

To evaluate the efficacy of the proposed acceleration-based slip detection logic, an accurate representation of wheel speed sensor noise is paramount. To establish a baseline, the 5-DoF vehicle model was subjected to a smooth rear-wheel torque demand, defined as $M_R = 50(\tanh(2(t-5))+1)\,\text{N}\cdot\text{m}$ with zero torque applied to the front axle. As shown in Figure 2, this generates a smooth transient angular velocity profile for both the driven and non-driven wheels without inducing deep slip.

To reflect physical hardware, normally distributed white noise was injected into this clean velocity signal (Figure 3). Deriving angular acceleration from this raw, noisy velocity via a basic first-order backward finite difference yields an entirely unusable signal. As demonstrated in Figure 4, the numerical differentiation violently amplifies the high-frequency quantization noise, completely masking the true physical acceleration and rendering any threshold-based detection impossible.

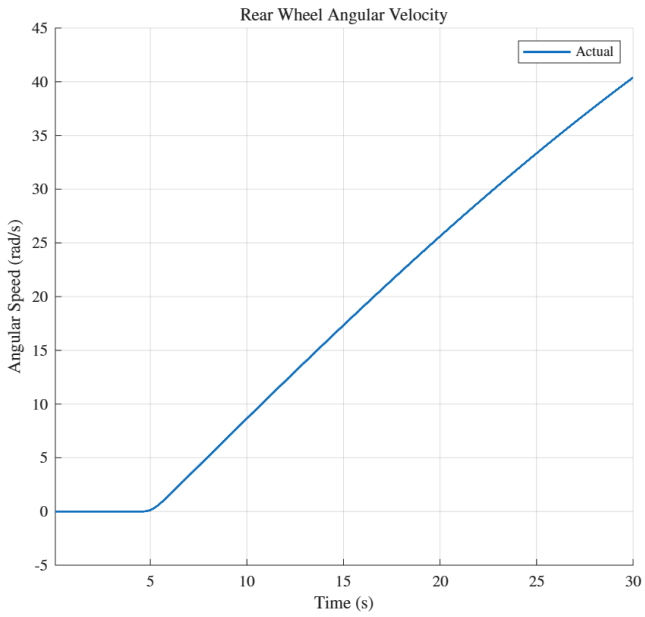


Fig. 2. Clean Angular Velocity

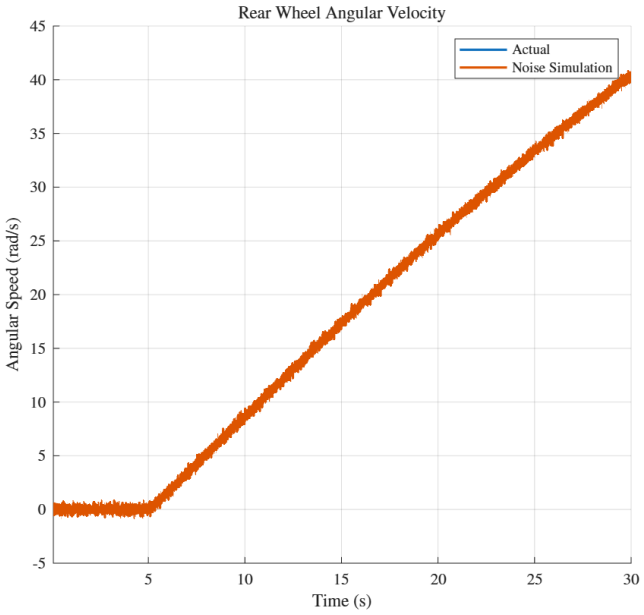


Fig. 3. Noisy Angular Velocity

Several intermediate filtering methodologies were evaluated to recover the true acceleration signal. Initially, a standard two-state Kinematic Kalman Filter was utilized in isolation [6]. While this attenuated the noise marginally, the residual high-frequency variance remained too large for stable control without severe detuning, which induced unacceptable phase lag (Figure 5). Subsequent iterations paired the Kalman Filter with discrete Finite Impulse Response (FIR) low-pass filters. While the signal smoothness improved, FIR filters inherently impose a linear phase delay, delaying the controller's reaction time to slip events [12].

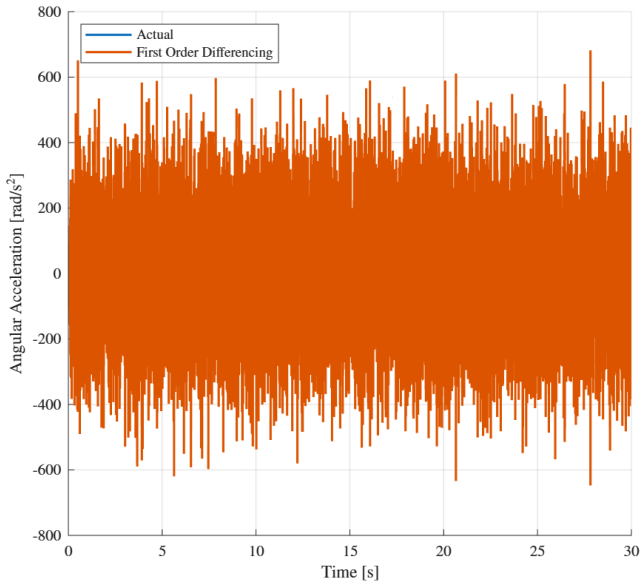


Fig. 4. Raw Finite Difference Acceleration

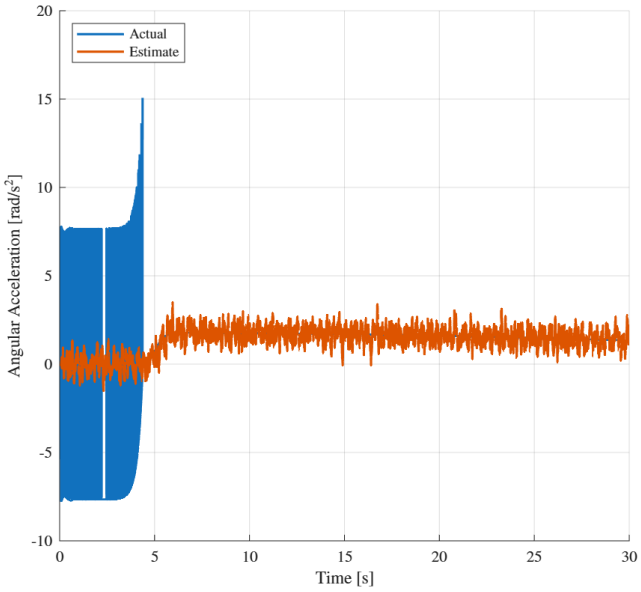


Fig. 5. Kalman Filter Output

During the initial phase of the simulation, the estimated angular acceleration signal exhibits high-frequency oscillations and numerical "chattering." This behavior is caused by a mathematical singularity inherent in the longitudinal slip ratio calculation, where the denominator (longitudinal velocity) approaches zero. Although a small tolerance constant (ϵ_{tol}) is employed to prevent division by zero, the high sensitivity of the tire force equations at near-zero speeds results in transient numerical uncertainty. Once the vehicle surpasses a nominal velocity threshold ($> 0.1\,\mathrm{m/s}$), the kinematic states stabilize, and the signal processing pipeline successfully recovers a smooth, physically consistent acceleration profile.

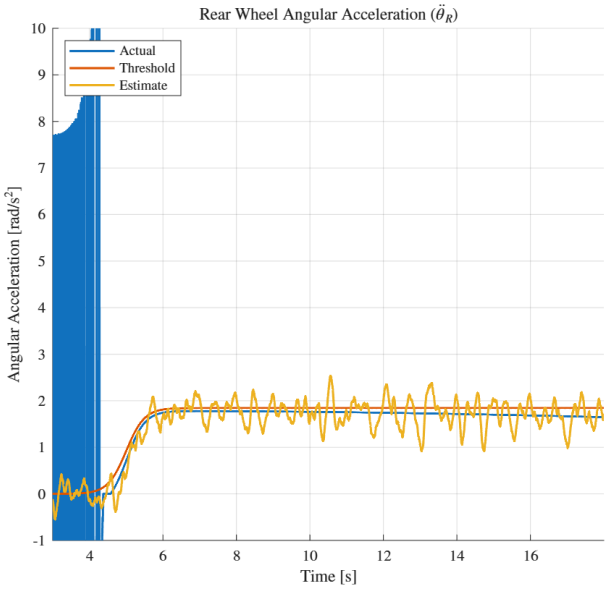


Fig. 6. Final 3-Stage Pipeline Output

Further experimentation explored Augmented Kalman Filters designed to track and cancel structured noise dynamically. Although these augmented architectures successfully reduced

noise during steady-state operation, they exhibited mathematical instability during transient events. When subjected to sudden step-changes in torque, the augmented filters produced anomalous acceleration spikes that significantly deviated from the known physical values, precluding their use as a reliable trigger for safety systems.

Ultimately, the three-stage pipeline consisting of a Kinematic Kalman filter, a Causal Savitzky-Golay polynomial fit [7], and a Statistical Shrinkage Estimator [8] proved superior. As illustrated in Figure 6, this experimental pipeline successfully attenuates the high-frequency noise while inducing only an acceptable, minimal phase lag, allowing the estimated acceleration to track the physical threshold reliably.

B. Controller Performance and Tuning (RWD)

With a stabilized acceleration estimate established, the feedback control strategy was iteratively tested on a Rear-Wheel Drive (RWD) configuration. The vehicle was subjected to an aggressive torque demand intended to break traction on a low-friction surface ($\mu = 0.25$). The input torque was defined as $M_R = 110.5(\tanh(2(t-5))+1) - -55.25(\tanh(2(t-15))+1)\,\mathrm{N}\cdot\mathrm{m}$. The first implementation utilized a purely Proportional (P) controller acting on the threshold error. As shown in Figure 7 and Figure 8, while the P-controller successfully arrested the runaway wheel slip and maintained gross system stability, it exhibited a fundamental limitation: a persistent steady-state offset [13]. The controlled angular acceleration consistently remained above the physical friction limit, allowing the angular velocity to continue into deep slip.

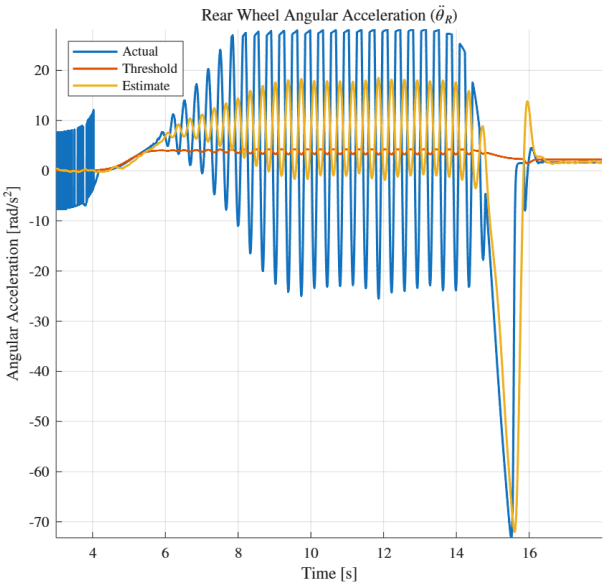


Fig. 7. P-Controller Angular Acceleration Response

To eliminate this tracking error, an Integral (I) term was introduced. As illustrated in Figure 9 and Figure 10, the resulting Proportional-Integral (PI) controller successfully compensated for the offset and forced the steady-state error to zero, ensuring the tire operated exactly at the boundary of peak friction.

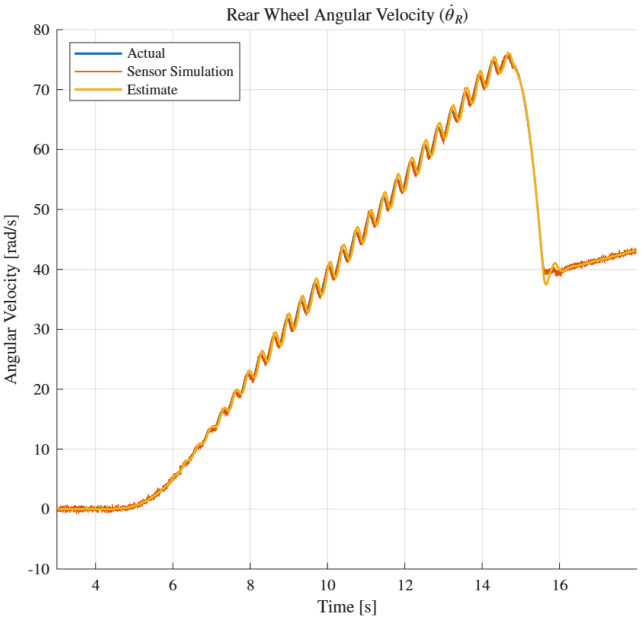


Fig. 8. P-Controller Angular Velocity Response

A Derivative (D) term was explicitly excluded from the architecture. Because the controller error signal is derived from angular acceleration, a derivative term would require calculating the numerical derivative of acceleration (i.e., angular jerk). Subjecting an already estimated, slightly noisy acceleration signal to further numerical differentiation would cause unbounded high-frequency command chatter, destroying control stability [11].

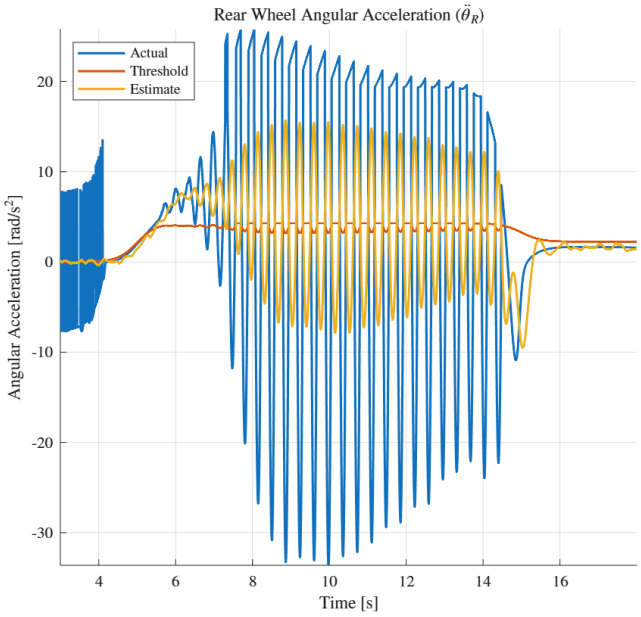


Fig. 9. Basic PI-Controller Acceleration Response

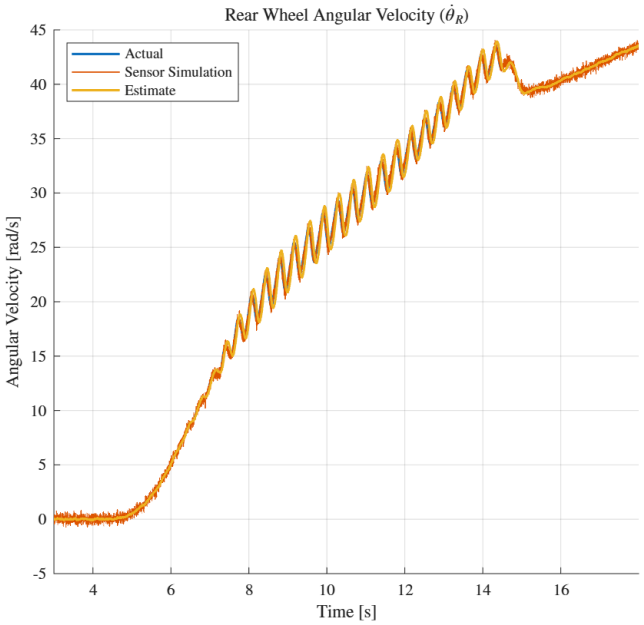


Fig. 10. Basic PI-Controller Velocity Response

Finally, the addition of the asymmetric slew-rate limiter eliminated the destructive, high-frequency "bang-bang" chatter present in early PI iterations. The final controller responses (Figure 11 and Figure 12) demonstrate a rapid, near-instantaneous torque reduction upon slip detection, followed by a smooth, slew-limited torque recovery, maximizing passenger comfort and mechanical reliability.

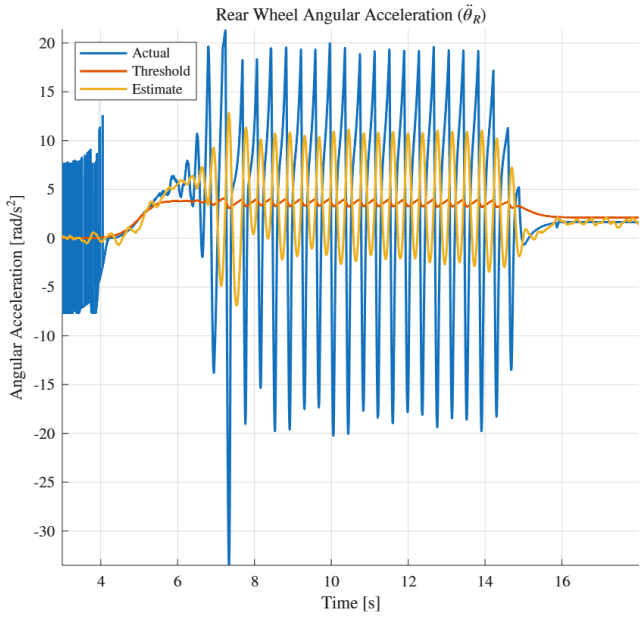


Fig. 11. Slew PI-Controller Acceleration Response

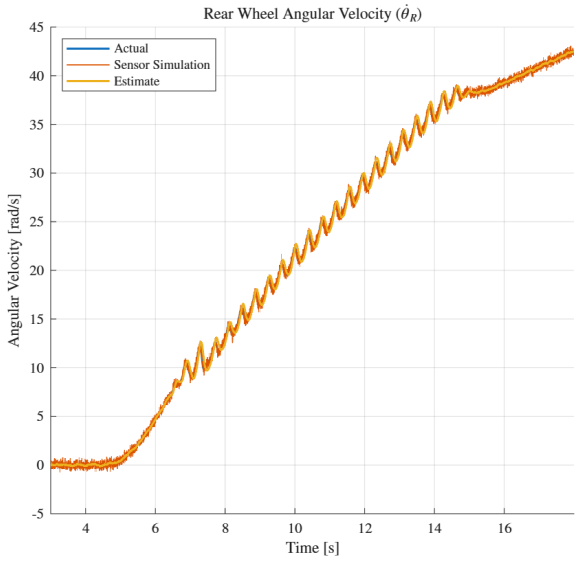


Fig. 12. Slew PI-Controller Velocity Response

C. All-Wheel Drive (AWD) Implementation

To validate the robustness of the decentralized control logic, the simulation was expanded to an All-Wheel Drive (AWD) vehicle with a 50/50 static power split. The driver input functions for the front and rear axles were defined symmetrically as $M_F = M_R = 103.5(\tanh(2(t-5))+1) - 50(\tanh(2(t-15))+1)$. As dynamic load transfers to the rear axle during acceleration, the front axle's normal force decreases, causing its angular acceleration to increase more than the rear wheel's angular acceleration. As demonstrated in Figure 13 to Figure 16, the independent controllers successfully identify the distinct thresholds for both the front and rear wheels simultaneously. The front controller actively mitigates slip more aggressively than the rear, proving that the velocity-independent acceleration threshold methodology functions reliably across multi-axle drivelines experiencing transient load transfer.

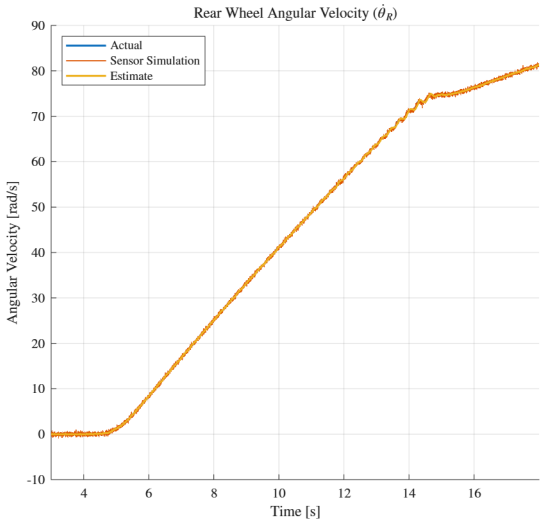


Fig. 13. AWD Rear Axle Velocity

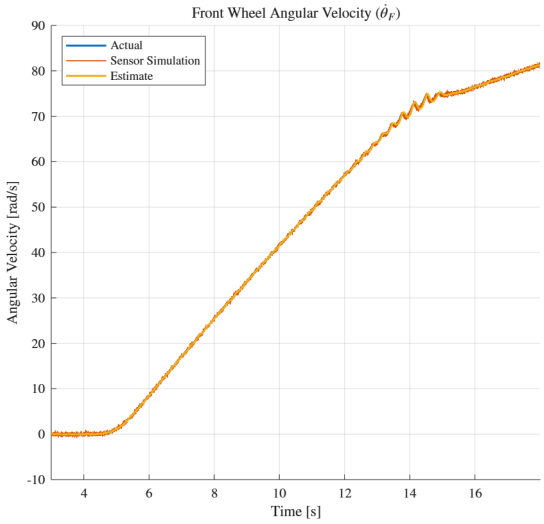


Fig. 14. AWD Front Axle Velocity

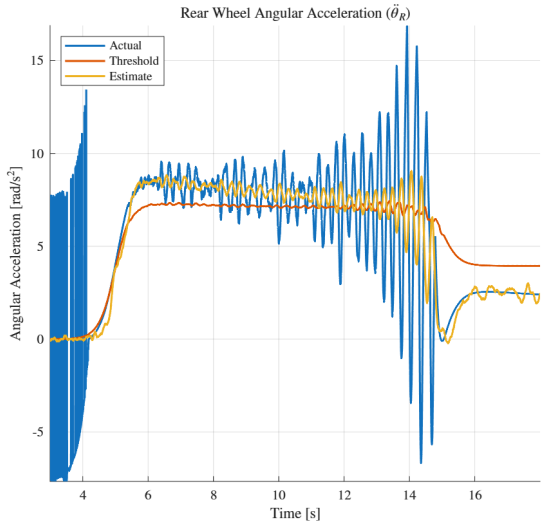


Fig. 15. AWD Rear Axle Acceleration

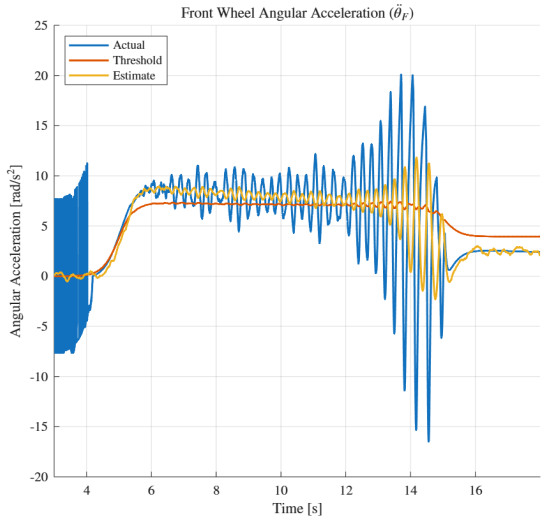


Fig. 16. AWD Front Axle Acceleration

VI. Conclusion

This paper presented a robust, velocity-independent traction control architecture that mitigates longitudinal wheel slip by relying on physical wheel angular acceleration thresholds. By decoupling the control logic from longitudinal vehicle speed estimates, the proposed system eliminates the unreliability inherent in traditional slip-ratio-based systems during deep or all-wheel slip events.

To accurately establish these dynamic acceleration limits, a 5-DoF half-car model was coupled with a nonlinear Pacejka tire model, successfully capturing the critical effects of dynamic load transfer on peak tractive capability. The violent amplification of high-frequency sensor noise via numerical differentiation was resolved through a custom three-stage discrete-time signal processing pipeline. The pipeline produced a usable acceleration signal without introducing prohibitive phase lag.

Furthermore, the implementation of a decentralized, asymmetric Proportional-Integral (PI) controller equipped with an anti-windup clamp and slew-rate limiting effectively suppressed destructive mechanical chatter. Simulation results across both drivetrain configurations on low-friction surfaces validated the methodology. The independent controllers accurately tracked shifting friction thresholds caused by transient load transfer, executing near-instantaneous torque reductions followed by smooth, slew-limited recoveries.

Ultimately, this velocity-independent framework demonstrates that continuous longitudinal acceleration can be safely maximized relying solely on wheel speed sensors. Future work will explore the integration of adaptive gain scheduling to manage rapid surface friction transitions ("μ-jump" scenarios) and experimental validation on a physical hardware platform.

References

[1] R. Rajamani, *Vehicle Dynamics and Control*, 2nd ed. New York, NY, USA: Springer, 2012.
[2] S. M. Savaresi and M. Tanelli, *Active Braking Control Systems Design for Vehicles*. London: Springer-Verlag, 2010.
[3] H. B. Pacejka, *Tire and Vehicle Dynamics*. Amsterdam: Elsevier, 2006.
[4] SAE International, *Vehicle Dynamics Terminology*, SAE Standard J670, 2008.
[5] M. I. Galicia, J. D. Sánchez, A. G. Loukianov, and J. Rivera, "Sliding Mode Control for Antilock Brake System," in *2010 7th International Conference on Electrical Engineering, Computing Science and Automatic Control (CCE)*, Tuxtla Gutiérrez, Mexico, 2010.
[6] R. E. Kalman, "A New Approach to Linear Filtering and Prediction Problems," *Journal of Basic Engineering*, vol. 82, no. 1, pp. 35-45, 1960.
[7] A. Savitzky and M. J. E. Golay, "Smoothing and Differentiation of Data by Simplified Least Squares Procedures," *Analytical Chemistry*, vol. 36, no. 8, pp. 1627-1639, 1964.
[8] G. James, D. Witten, T. Hastie, and R. Tibshirani, *An Introduction to Statistical Learning*, New York: Springer, 2013.
[9] K. Ogata, *Modern Control Engineering*, 5th ed. Upper Saddle River, NJ, USA: Prentice Hall, 2010.
[10] F. Borrelli, A. Bemporad, and M. Morari, *Predictive Control for Linear and Hybrid Systems*. Cambridge, U.K.: Cambridge University Press, 2017.
[11] G. F. Franklin, J. D. Powell, and M. L. Workman, *Digital Control of Dynamic Systems*, 3rd ed. Menlo Park, CA, USA: Addison-Wesley, 1998.
[12] A. V. Oppenheim and R. W. Schafer, *Discrete-Time Signal Processing*, 3rd ed. Upper Saddle River, NJ, USA: Pearson, 2009.
[13] K. J. Åström and T. Hägglund, *PID Controllers: Theory, Design, and Tuning*, 2nd ed. Research Triangle Park, NC, USA: ISA, 1995.